

# Identifying structural patterns in ‘disordered’ metal clusters

Jonathan P. K. Doye\*

*University Chemical Laboratory, Lensfield Road, Cambridge CB2 1EW, United Kingdom*

(Dated: February 2, 2008)

Zinc and cadmium clusters interacting with a Gupta potential have previously been identified as prototypical metallic systems that exhibiting disordered cluster structures. Here, putative global minima of the potential energy have been located for these clusters for all sizes up to  $N \leq 125$ . Although none of the usual structural forms are lowest in energy and many of the clusters have no overall order, strong structural preferences have been identified. Many of the clusters are based on distorted oblate Marks decahedra, where the distortion involves the bringing together of atoms on either side of a re-entrant groove of the Marks decahedron.

## I. INTRODUCTION

There has been much recent theoretical interest in the possibility that small clusters could have lowest-energy structures that are disordered or amorphous. Examples have been found for model clusters interacting with long-ranged pair potentials,<sup>1,2</sup> and a wide variety of metal clusters.<sup>3,4,5,6,7,8,9,10,11,12,13,14,15,16</sup> For some of these examples, these disordered clusters appear at sizes between the magic numbers for the usual icosahedral, decahedral or face-centred-cubic (fcc) forms, that are typically most stable for materials that are close-packed for bulk;<sup>10,13,14,15</sup> i.e. the disordered structures are more stable than ordered structures with incomplete outer layers. More interesting are the more extreme examples, where disordered structures are lowest in energy even at the magic numbers of the common structural forms.<sup>3,4,7,8</sup> These results would suggest for these clusters that the disordered structures are dominant for the relevant size ranges.

By disordered it is usually meant that the structure has no discernible overall order. Of course, there is still local order, as evidenced by structural probes, such as the radial distribution function, but these usually have forms similar to that for bulk liquids and glasses. Additionally, another common features for these clusters is that there are many other disordered structures that lie very close in energy to the global minimum.

Disordered clusters are most likely to occur when the constraints on the nearest-neighbour distances are weak. Then, the energetic cost for the strain present in the individual nearest-neighbour bonds can be low enough to be offset by other advantageous features of the disordered clusters, such as a low surface energy. For the Morse clusters, this occurs when the potential is long-ranged and has a wide, soft well.<sup>1,2</sup> For metal clusters, the many-body part of the potential is relatively insensitive to disorder in the nearest-neighbour distances.<sup>17</sup> If the contraction at the surface of the cluster (again due to the many-body forces) is strong, the ordered structures can be sufficiently destabilized to make the disordered structures lowest in energy.<sup>17</sup>

For most of the examples where disordered structures have been found to be lower in energy than the most sta-

ble icosahedral, decahedral and fcc clusters, only a few sizes have usually been considered.<sup>3,4,7,8</sup> So, the possibility remains that at some other sizes the local structural preferences present in the disordered clusters could be assembled in a way that gives rise to a particularly stable structure with overall order. If this were the case, global optimization over a complete range of sizes would then reveal these new structural motifs and magic numbers. This has recently been done for model lead clusters, where, although none of the usual forms are ever lowest in energy and many of the clusters have no apparent overall order, particularly stable high-symmetry clusters were found at some sizes.<sup>11</sup>

Indeed there are general grounds for expecting high symmetry structures to be more prevalent among the global minima, because such structures are likely to have more extreme values of the energy (both high and low).<sup>18</sup> This expectation, in my experience at least, seems to be born out empirically. It is rare that the global optimization of clusters does not reveal ordered high symmetry forms at some sizes. For example, even for potentials which have been designed to favour glassy configurations, global optimization has revealed the presence of unusual, but nevertheless ordered, structures.<sup>19,20</sup>

Here, I wish to examine some prototypical metal clusters that so far have only been found to exhibit disordered structures. For potentials of the Gupta form the dependence of the tendency to disorder on some of the parameters of the potential has been elaborated.<sup>4,17</sup> Of the parameterized metals zinc and cadmium clusters emerged as those with the strongest preference for disorder. This tendency was born out in global optimization studies at sizes where particularly stable fcc, decahedral and icosahedral structures were possible; as expected, the resulting structures appeared disordered.<sup>7</sup>

In this paper, I will attempt to identify structural patterns for these two cluster systems, in particular searching for new magic numbers and novel types of order. This aim is in a similar spirit to Ref. 21, where possible structural patterns for gold clusters modelled by the Gupta potential have been suggested. To achieve this I have performed global optimization for all clusters with up to 125 atoms. A further aim is to then relate back the identified structural patterns to the form of the potential.

TABLE I: Parameters for the Gupta potentials of Zn and Cd.

	$p$	$q$	$A / \text{eV}$	$\xi / \text{eV}$
Zn	9.689	4.602	0.1477	0.8900
Cd	10.612	5.206	0.1420	0.8117

## II. METHODS

### A. Potential

To model the zinc and cadmium clusters I use a Gupta potential<sup>22</sup> fitted by Cleri and Rosato.<sup>23</sup> The potential energy is given by

$$E = E_{\text{pair}} + E_{\text{embed}} \quad (1)$$

$$= \sum_{i < j} \phi(r_{ij}) + \sum_i F(\bar{\rho}_i), \quad (2)$$

where  $\phi(r)$  is a short-ranged pair potential,  $U(\bar{\rho})$  is a many-body embedding (or glue) function and  $\bar{\rho}_i$  is defined as

$$\bar{\rho}_i = \sum_j \rho(r_{ij}), \quad (3)$$

where  $\rho(r)$  is an ‘‘atomic density’’ function.

For potentials of the Gupta form

$$\phi(r) = 2Ae^{-p(r/r_0-1)} \quad (4)$$

$$F(\bar{\rho}) = -\xi\sqrt{\bar{\rho}} \quad (5)$$

$$\rho(r) = e^{-2q(r/r_0-1)}. \quad (6)$$

These forms arise from the second moment approximation of a tight-binding Hamiltonian. However, these functions are non-unique. Functions that give exactly the same energy can be constructed by the transformation

$$\phi'(r) = \phi(r) + 2g\rho(r) \quad (7)$$

$$F'(\bar{\rho}) = F(\bar{\rho}) - g\bar{\rho}. \quad (8)$$

This transformation redistributes the total energy between  $E_{\text{pair}}$  and  $E_{\text{embed}}$ . When

$$g = \left. \frac{dF}{d\bar{\rho}} \right|_{\bar{\rho}=\bar{\rho}_{\text{xtal}}}, \quad (9)$$

$F'(\bar{\rho})$  has a minimum at  $\bar{\rho}_{\text{xtal}}$ , where  $\bar{\rho}_{\text{xtal}}$  is the value of  $\bar{\rho}$  in the equilibrium crystal. This choice is called the effective pair format, and has been suggested as the most natural way to partition the energy between the pair and many-body contributions.<sup>24</sup> In this format, when  $\bar{\rho} = \bar{\rho}_{\text{xtal}}$  the pair potential controls the energy change for any change of configuration that does not significantly alter  $\bar{\rho}$ , hence the name. More specifically, by performing a Taylor expansion about this reference density, one can show that to first order, the change in energy is due to

the pair potential. Consequently, it is also a much more helpful format for relating the structure to the form of the potential.

The Gupta potential in this effective pair format becomes

$$\phi_{\text{eff}}(r) = 2Ae^{-p(r/r_0-1)} - \frac{\xi}{\sqrt{\bar{\rho}_{\text{xtal}}}} e^{-2q(r/r_0-1)} \quad (10)$$

$$F_{\text{eff}}(\bar{\rho}) = -\xi\sqrt{\bar{\rho}} \left( 1 - \frac{1}{2} \sqrt{\frac{\bar{\rho}}{\bar{\rho}_{\text{xtal}}}} \right). \quad (11)$$

$\phi_{\text{eff}}(r)$  is a sum of two exponentials, so for  $p > 2q$  it is repulsive at short range and has an attractive well. The minimum in  $\phi_{\text{eff}}(r)$  is at

$$r_{\text{min}} = r_0 \left( 1 + \frac{1}{p-2q} \log \left( \frac{Ap\sqrt{\bar{\rho}_{\text{xtal}}}}{\xi q} \right) \right) \quad (12)$$

and is of depth

$$\phi_{\text{eff}}(r_{\text{min}}) = -A \left( \frac{\xi q}{Ap\sqrt{\bar{\rho}_{\text{xtal}}}} \right)^{p/p-2q} \left( \frac{p-2q}{q} \right) \quad (13)$$

As  $p \rightarrow 2q$  from above, the depth of the well in the pair potential goes to zero.  $F_{\text{eff}}(\bar{\rho})$  is quadratic in  $\sqrt{\bar{\rho}}$  and has a minimum of depth  $-\xi\sqrt{\bar{\rho}_{\text{xtal}}}/2$  at  $\bar{\rho} = \bar{\rho}_{\text{xtal}}$ .

The Gupta parameters for the Zn and Cd potentials are given in Table I, and the functions  $\phi_{\text{eff}}$ ,  $\rho$  and  $F_{\text{eff}}$  are shown in Fig. 1. The shallowness of the attractive well in the effective pair potential of cadmium is particularly apparent—it is only 0.26% of the depth of the minimum in the embedding function. The pair well depth is somewhat larger for zinc, but it is still only 0.70% of the embedding function minimum. For both systems the shallowness arises because  $p/q$  is close to 2.

This feature of the potentials will have similar structural consequences for both systems. Firstly, the majority of the binding energy will come from the many-body interactions. Secondly, the pair potential provides relatively little constraint on the pair distances, except for the repulsion at short distances. Therefore, the most important feature for obtaining a low-energy configuration is to have the individual  $\bar{\rho}_i$  values as close as possible to the optimal value. By contrast, there is little energetic advantage in having the nearest-neighbour distances close to the minimum of the pair potential. For a cluster the former can sometimes be more easily achieved through a disordered structure than one based on a lattice, because the additional flexibility of not having well-defined nearest-neighbour distances makes it easier to obtain close to optimal  $\bar{\rho}$  values for the surface atoms. This is the source of the tendency to disorder for zinc and cadmium clusters described by the current potentials.

For bulk both zinc and cadmium are hexagonal close-packed with  $\bar{\rho}_{\text{xtal}}^{\text{Cd}} = 8.042$ , and  $\bar{\rho}_{\text{xtal}}^{\text{Zn}} = 8.638$ . These are anomalously low values for close-packed materials. For example, for an ideal close-packed crystal with all nearest-neighbours at  $r_0$ , the nearest-neighbour contribution to  $\bar{\rho}$  is 12. However, the ratios of the unit cell

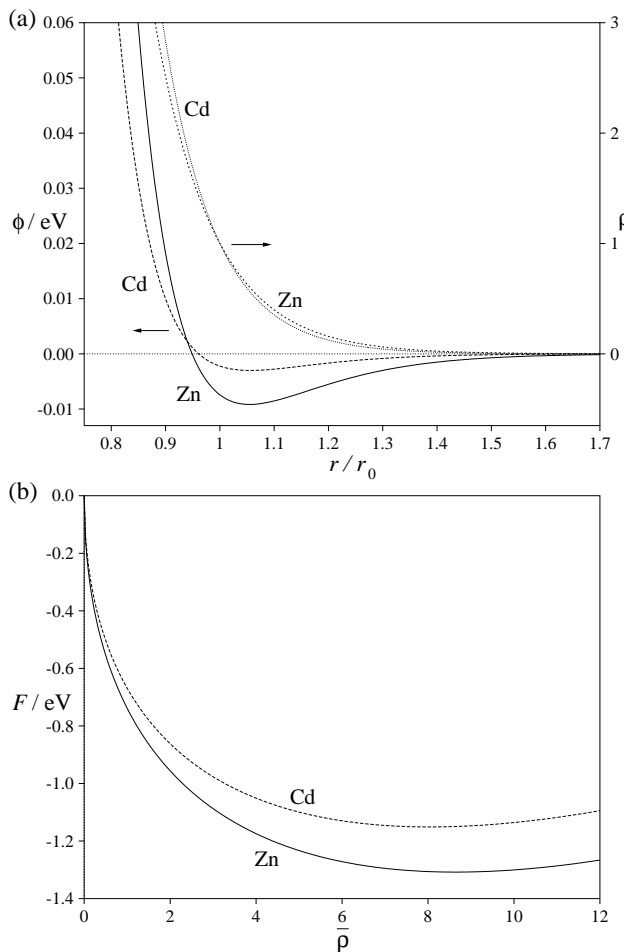


FIG. 1: The three functions that make up the potential: (a)  $\phi_{\text{eff}}(r)$ ,  $\rho(r)$  and (b)  $F_{\text{eff}}(\bar{\rho})$ .

parameters  $c/a$  for the Zn and Cd crystals are particularly large, and so the contribution to  $\bar{\rho}$  from nearest-neighbour distances with a component in the  $c$  direction is significantly reduced.

The low values of  $\bar{\rho}_{\text{xtal}}$  have structural consequences for the clusters. An atom can achieve the optimal  $\bar{\rho}$  values with only eight or nine neighbours, so this is possible for surface atoms. By contrast, the nearest-neighbour distances for atoms in the interior need to be elongated to prevent unfavourably large values of  $\bar{\rho}$ . This is bad news for cluster structures, such as the Mackay icosahedron, where the interior distances are naturally shorter than those on the surface.

The exponential nature of  $\rho(r)$  means that significant changes to the  $\bar{\rho}$  values can be achieved by relatively small changes to the nearest-neighbour distances. Consequently, it is somewhat easier for atoms, even those with low coordination numbers, to obtain nearly optimal  $\bar{\rho}$  values. This behaviour contrasts with other many-body potential, for instance those produced by the force-matching method,<sup>25</sup> where there is no presumed form for  $\rho(r)$ , and so more long-ranged functions can result.<sup>25,26,27</sup>

The current potentials were obtained by keeping the  $c/a$  value fixed at the experimental value. This is at some cost in terms of the quality of the fit to other quantities. This led Cleri and Rosato to also construct potentials in which the  $c/a$  ratio was allowed to vary in the fitting procedure, and resulted in a better quality fit for many properties.<sup>23</sup> Such a potential is available for cadmium and has dramatically different structural properties because  $p/q = 3.49$ .

## B. Global Optimization

The global optimization of the zinc and cadmium clusters was performed using the basin-hopping<sup>28,29</sup> (or Monte Carlo minimization<sup>30</sup>) approach. This method has proved particularly successful in locating putative global minima for a wide variety of cluster systems. The nature of the potentials for the current clusters, particularly that  $p - 2q$  is small, makes global optimization difficult compared to many other metal clusters of similar size. Therefore, a considerable computational effort was required to extend the results up to 125 atoms. It proved particularly important to supplement the standard unbiased runs from random starting points for each size, with short runs started from low-energy minima of nearby sizes with the appropriate number of atoms added or removed. As the structures of the two clusters are similar—seventy of the global minima are the same—it also proved useful to reoptimize the low-energy minima found for one metal for the other. These two types of ‘seeded’ runs were applied iteratively until no further new global minima were located.

It should be noted that, of course, there is no guarantee that I have been able to locate the true global minima, and the probability that a global minimum has been missed will increase with cluster size, as the size of the search space, and hence the number of minima,<sup>31,32,33</sup> increases exponentially with  $N$ . Examination of the statistics of how often independent runs locate the same lowest-energy minimum and the importance of the seeded runs can provide one with an idea of the likelihood that the true global minimum has been found. For example, for zinc clusters with less than ninety atoms virtually all the putative global minima were located in unbiased runs, but for  $N > 100$  the majority of putative global minima were only located in seeded runs. Similarly, for the cadmium clusters virtually all the putative global minima were only located in seeded runs for  $N \geq 65$ . This greater difficulty is because  $2p - q$  is closer to zero for cadmium. However, given the similarity of the observed structures for the two metals, I am confident that the vast majority of the putative global minima up to  $N = 100$  cannot be bettered, but beyond this size one’s degree of scepticism about the success of the global optimization should increase rapidly.

TABLE II: Energies (in eV) and point groups of putative  $Zn_N$  global minima

$N$	PG	Energy	$N$	PG	Energy	$N$	PG	Energy	$N$	PG	Energy	$N$	PG	Energy
3	$D_{3h}$	-3.751296	28	$D_{6d}$	-37.076416	53	$C_1$	-70.622509	78	$C_1$	-104.238674	103	$C_1$	-137.902829
4	$T_d$	-5.099346	29	$C_2$	-38.410947	54	$C_1$	-71.969642	79	$C_{2v}$	-105.595357	104	$C_1$	-139.255744
5	$D_{3h}$	-6.422287	30	$C_1$	-39.768212	55	$C_1$	-73.310032	80	$C_{2v}$	-106.927940	105	$C_1$	-140.593303
6	$O_h$	-7.765873	31	$C_1$	-41.107234	56	$C_1$	-74.649595	81	$C_s$	-108.284296	106	$C_1$	-141.928489
7	$D_{5h}$	-9.088519	32	$C_1$	-42.444864	57	$C_1$	-75.992628	82	$C_s$	-109.625208	107	$C_1$	-143.279843
8	$D_{2d}$	-10.409083	33	$C_1$	-43.776617	58	$C_1$	-77.336947	83	$C_s$	-110.976689	108	$C_1$	-144.635048
9	$C_{2v}$	-11.733002	34	$C_3$	-45.125218	59	$C_1$	-78.672227	84	$C_s$	-112.322650	109	$C_1$	-145.978993
10	$C_{3v}$	-13.055156	35	$C_s$	-46.472931	60	$C_1$	-80.019432	85	$C_1$	-113.668080	110	$C_1$	-147.337545
11	$C_2$	-14.379679	36	$D_{2h}$	-47.814946	61	$C_2$	-81.363067	86	$C_{2v}$	-115.021815	111	$C_2$	-148.697585
12	$C_2$	-15.706971	37	$C_1$	-49.144718	62	$C_1$	-82.708058	87	$C_{2v}$	-116.375101	112	$C_1$	-150.033337
13	$C_s$	-17.032142	38	$C_s$	-50.499983	63	$C_1$	-84.061400	88	$C_{2v}$	-117.726908	113	$C_1$	-151.385243
14	$C_{6v}$	-18.369312	39	$C_{2v}$	-51.846864	64	$C_2$	-85.419385	89	$C_s$	-119.057698	114	$C_1$	-152.720206
15	$C_s$	-19.697479	40	$C_s$	-53.182148	65	$C_1$	-86.749702	90	$C_s$	-120.405576	115	$C_2$	-154.071651
16	$C_s$	-21.042019	41	$C_s$	-54.521834	66	$C_1$	-88.097872	91	$C_{2v}$	-121.767147	116	$C_1$	-155.420956
17	$C_{2v}$	-22.395676	42	$D_4$	-55.874358	67	$C_1$	-89.426800	92	$C_{2v}$	-123.118340	117	$C_1$	-156.762711
18	$C_{4v}$	-23.735972	43	$C_4$	-57.213737	68	$C_1$	-90.782264	93	$C_s$	-124.451825	118	$C_1$	-158.109816
19	$D_{4d}$	-25.067563	44	$C_s$	-58.554345	69	$C_1$	-92.135925	94	$C_s$	-125.796431	119	$C_1$	-159.451202
20	$C_{2v}$	-26.395373	45	$C_{2v}$	-59.895318	70	$C_1$	-93.473840	95	$C_s$	-127.142167	120	$C_{2v}$	-160.812498
21	$C_s$	-27.715028	46	$C_s$	-61.227348	71	$C_s$	-94.828826	96	$C_{2v}$	-128.501419	121	$C_1$	-162.152965
22	$C_{2v}$	-29.042499	47	$C_s$	-62.580198	72	$C_s$	-96.168254	97	$C_s$	-129.836679	122	$C_1$	-163.502185
23	$C_1$	-30.386460	48	$C_s$	-63.916581	73	$C_s$	-97.513085	98	$C_{2v}$	-131.170669	123	$C_{2v}$	-164.859277
24	$C_2$	-31.728122	49	$C_{2v}$	-65.269233	74	$C_s$	-98.853247	99	$C_s$	-132.525475	124	$C_1$	-166.196591
25	$C_2$	-33.075590	50	$C_s$	-66.601903	75	$C_{2v}$	-100.203580	100	$C_{2v}$	-133.883827	125	$C_1$	-167.548063
26	$C_2$	-34.412179	51	$C_1$	-67.938575	76	$C_1$	-101.545341	101	$C_s$	-135.219057			
27	$C_2$	-35.744950	52	$C_{2v}$	-69.281361	77	$C_s$	-102.900278	102	$C_1$	-136.566429			

### III. GLOBAL MINIMA

The energies and point groups for the putative global minima are given in Tables II and III. Point files are available online at the Cambridge Cluster Database.<sup>34</sup> The energies of the global minima are represented in Fig. 2 in such a way that makes particularly stable clusters stand out.

The previous results for these clusters were for a selection of sizes that often show highly symmetric structures, namely  $N = 13, 38, 55$  and  $147$ .<sup>7</sup> For  $N=13$  and  $38$  the three lowest-energy minima reported in Ref. 7 agree with the current results. However, for  $Zn_{55}$ ,  $Zn_{75}$  and  $Cd_{75}$  the lowest-energy structures reported by Michaelian *et al.* correspond at best to the third, eighth, and twenty-second lowest-energy minima, respectively, and lie 0.0031, 0.0186 and 0.0086 eV above the lowest-energy minima reported here. These energies are significant compared to the variations shown in Fig. 2. I did not systematically attempt to optimize 147-atom clusters, as locating the true global minimum for this size would be extremely difficult. However, short basin-hopping runs did find structures that were 0.0966 and 0.0304 eV lower in energy for  $Zn_{147}$  and  $Cd_{147}$ , respectively, than the

lowest-energy structures found by Michaelian *et al.*<sup>7</sup>

Before, we examine the observed structures, there are a number of interesting features evident from Fig. 2. The energy zero in these figures is  $E_{ave}$ , a four-parameter fit to the energies of the global minima, where the first two terms correspond to volume and surface energies. For these two clusters the surface term is exceptionally small. The ratio of the surface to the volume coefficient is 7.8% for Zn and 3.3% for Cd. For comparison the value of this ratio is 197% for Lennard-Jones clusters,<sup>35</sup> 48% for Gupta lead clusters,<sup>36,37</sup> 60% for aluminium clusters,<sup>38</sup> and 93%, 87% and 63% for Sutton-Chen silver, nickel and gold clusters, respectively<sup>10</sup>. One expects the surface energy to be lower for metal clusters than for a cluster interacting with a pair potential, because the lower coordinate surface atoms of a metal can increase their many-body embedding energy by shortening their nearest neighbour distances. But the Zn and Cd surface energies are very low even for metals, because the optimal value of  $\bar{\rho}$  is small enough to be achievable by the surface atoms and the effective pair potential only makes a small contribution to the energy.

The second interesting feature is the magnitude of the fluctuations about the average energy. For Cd and Zn

TABLE III: Energies (in eV) and point groups of putative  $\text{Cd}_N$  global minima. Those labelled with a star have the same structure as the  $\text{Zn}_N$  global minimum.

$N$	PG	Energy	$N$	PG	Energy	$N$	PG	Energy	$N$	PG	Energy	$N$	PG	Energy				
3	$D_{3h}$	-3.391649	*	28	$C_2$	-32.354453	53	$C_1$	-61.383718	78	$C_1$	-90.441924	*	103	$C_1$	-119.516811	*	
4	$T_d$	-4.556244	*	29	$C_1$	-33.511796	54	$C_1$	-62.547483	79	$C_{2v}$	-91.609644	*	104	$C_1$	-120.682922	*	
5	$D_{3h}$	-5.710992	*	30	$C_2$	-34.677431	55	$C_s$	-63.711040	80	$C_s$	-92.767096	105	$C_1$	-121.841138			
6	$O_h$	-6.873544	*	31	$C_1$	-35.838691	*	56	$C_2$	-64.871474	81	$C_s$	-93.931045	*	106	$C_1$	-123.000416	*
7	$D_{5h}$	-8.028455	*	32	$C_1$	-36.999668	*	57	$C_1$	-66.031560	*	82	$C_1$	-95.092765	107	$C_1$	-124.164675	*
8	$D_{2d}$	-9.182587	*	33	$C_1$	-38.157466	*	58	$C_1$	-67.193590	83	$C_s$	-96.259818	*	108	$C_1$	-125.323742	
9	$C_{2v}$	-10.337961	*	34	$C_1$	-39.318659	59	$C_1$	-68.352805	*	84	$C_1$	-97.415006	109	$C_1$	-126.488046		
10	$D_{4d}$	-11.492834	35	$C_1$	-40.483344	60	$C_1$	-69.515486	85	$C_1$	-98.582433	*	110	$C_1$	-127.654226	*		
11	$C_2$	-12.648250	*	36	$D_{2h}$	-41.646892	*	61	$C_2$	-70.678373	*	86	$C_1$	-99.742283	111	$C_2$	-128.824065	*
12	$C_2$	-13.804680	*	37	$C_s$	-42.803277	62	$C_2$	-71.838429	87	$C_{2v}$	-100.912912	*	112	$C_1$	-129.985671	*	
13	$C_s$	-14.960307	*	38	$D_{2d}$	-43.967614	63	$C_1$	-73.002649	*	88	$C_{2v}$	-102.077956	*	113	$C_1$	-131.150549	*
14	$D_{6d}$	-16.116921	39	$C_{2v}$	-45.132103	*	64	$C_2$	-74.172601	*	89	$C_s$	-103.236780	*	114	$C_1$	-132.311215	*
15	$D_3$	-17.276238	40	$C_s$	-46.291870	*	65	$C_1$	-75.330653	90	$C_1$	-104.397182	115	$C_2$	-133.475490	*		
16	$C_s$	-18.434583	41	$C_{2v}$	-47.451405	66	$C_1$	-76.493660	*	91	$C_{2v}$	-105.565322	*	116	$C_1$	-134.637941	*	
17	$C_{2v}$	-19.600675	*	42	$D_4$	-48.613389	*	67	$C_1$	-77.650700	92	$C_{2v}$	-106.733237	*	117	$C_1$	-135.800525	*
18	$C_{2v}$	-20.764865	43	$C_4$	-49.774701	*	68	$C_1$	-78.815370	*	93	$C_s$	-107.892659	*	118	$C_1$	-136.963187	
19	$C_{2v}$	-21.923540	44	$C_s$	-50.937992	*	69	$C_1$	-79.982620	*	94	$C_s$	-109.048698	*	119	$C_1$	-138.125231	
20	$C_{2v}$	-23.080283	*	45	$C_{2v}$	-52.100346	*	70	$C_1$	-81.143066	*	95	$C_s$	-110.214298	120	$C_1$	-139.285228	
21	$C_1$	-24.234793	46	$C_s$	-53.258607	71	$C_1$	-82.302019	96	$C_s$	-111.382493	121	$C_2$	-140.450672				
22	$C_1$	-25.390380	47	$C_s$	-54.421794	*	72	$C_1$	-83.462242	97	$C_s$	-112.543725	*	122	$C_1$	-141.614397		
23	$C_1$	-26.552108	*	48	$C_s$	-55.581917	*	73	$C_s$	-84.623790	*	98	$C_s$	-113.703547	123	$C_{2v}$	-142.780180	*
24	$C_1$	-27.710728	49	$C_{2v}$	-56.746239	*	74	$C_s$	-85.787478	*	99	$C_s$	-114.863226	124	$C_1$	-143.938617		
25	$C_2$	-28.875894	*	50	$C_s$	-57.905181	*	75	$C_1$	-86.948788	100	$C_s$	-116.029828	125	$C_1$	-145.100610	*	
26	$C_2$	-30.036716	51	$C_1$	-59.063265	76	$C_1$	-88.112746	*	101	$C_s$	-117.191782	*					
27	$C_1$	-31.194825	52	$C_1$	-60.223182	77	$C_s$	-89.279311	*	102	$C_1$	-118.354639	*					

they are again exceptionally small. The average deviation from  $E_{\text{ave}}$  compared to the average energy per atom is 0.67% for Zn and 0.31% for Cd. For comparison, the value is 16% for Lennard-Jones clusters, 2.1% for Gupta lead clusters<sup>36,37</sup> and 5.6% for aluminium clusters<sup>38</sup> in the same size range.

The implications of these small fluctuations are that the differences between the more and less stable sizes indicated by Fig. 2 are small, making it more difficult to observe any such ‘magic’ numbers. Interestingly, one would expect that the properties of fully disordered clusters would evolve smoothly with size. By this measure, these zinc and cadmium clusters seem to be close to this limit.

We will first examine the zinc clusters in detail, and then later look at the relatively small structural difference between the two systems. A selection of zinc clusters are depicted in Fig. 3. that are either particularly stable or have some interesting structural feature. Up to  $N = 10$  the structure of the smallest zinc clusters are typical of what one usually finds for clusters modelled by empirical potentials. However, instead of structures leading up to the 13-atom icosahedra, more open structures are then preferred. The example shown in Fig. 3 for  $\text{Zn}_{13}$

can be considered as a polytetrahedral fragment of a 19-atom double icosahedron. It is insightful to examine, why this structure is lower in energy than the 13-atom icosahedron. The icosahedron is in fact 0.335 eV higher in energy, and this stems from an unfavourable embedding energy. The better pair energy, because of the icosahedron’s greater average coordination number, does little to offset this. As the distances between the central atom and the vertices of the icosahedron are 5% shorter than the distance between adjacent vertices and  $\rho(r)$  increases rapidly with decreasing  $r$ , the central atom has an extremely high value of  $\bar{\rho}$ , namely 19.568, that is much greater than the optimal value. By contrast, the  $\bar{\rho}$  values for all the atoms in the global minimum are relatively close to  $\rho_{\text{xtal}}$ . This is achieved by the atoms with low coordination number having shorter average distances.

This example illustrates two important features of the potential. First, low-coordinate surface atoms are not disfavoured, in contrast to a potential with a strong pair component. Second, it is important that interior atoms do not have short distances. As we will see, it is often much better for an interior atom to have a coordination number larger than twelve since then its nearest-neighbour distances will be longer than those between its

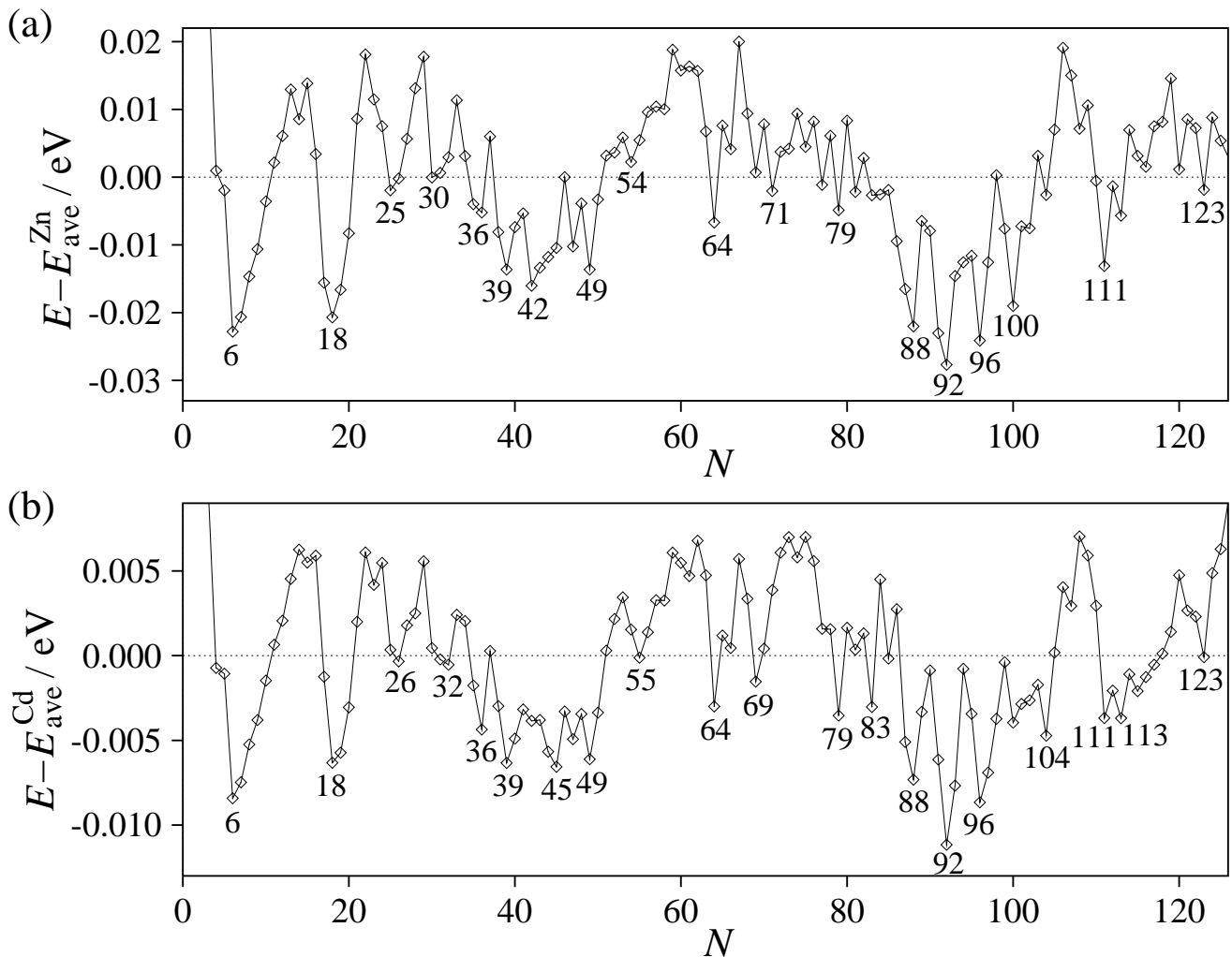


FIG. 2: Energies of the putative global minima of (a)  $\text{Zn}_N$  and (b)  $\text{Cd}_N$  relative to  $E_{\text{ave}}$ , a four-parameter fit to their energies.  $E_{\text{ave}}^{\text{Zn}} = -1.3621N + 0.1062N^{2/3} - 0.0067N^{1/3} + 0.0913$ .  $E_{\text{ave}}^{\text{Cd}} = -1.1684N + 0.0391N^{2/3} - 0.0143N^{1/3} + 0.0425$ .

neighbours. This latter feature is illustrated by the 14-atom global minimum. The 13-coordinate atom has an average nearest-neighbour separation of  $1.052 r_0$ , whereas the average separation for the nearest-neighbour contacts not involving this atom is  $0.958 r_0$ . Consequently  $\bar{\rho}$  for the central atom is only 10.381

The global minima for  $N=16-21$  can all be characterized as distorted decahedral structures. Decahedral structures are based on pentagonal bipyramids (hence the name) and have a single five-fold axis of symmetry. The pentagonal bipyramids themselves are usually not particularly stable because they have a relatively non-spherical shape. By the introduction of reentrant grooves at the five equatorial vertices that are parallel to the five-fold axis, more stable Marks decahedra can be produced.<sup>39,40</sup> An 18-atom example is shown in Fig. 4 that was derived from a 23-atom pentagonal bipyramid, where the introduction of the grooves gives rise to five four-coordinate capping atoms.

This 18-atom Marks decahedron is in fact itself not

that unstable and is only 0.042 eV above the global minimum. Even though the central atom is 12-coordinate, this atom is able to maintain a reasonable  $\bar{\rho}$  value (9.867), whilst an expansion of the structure along the axial direction allows the surface distances to contract.

However, the energy can be further improved by distorting this Marks decahedron. The distortion of this decahedra is easy to see for the 17-atom global minimum. This structure can be derived from the Marks decahedron (minus one capping one atom) by a diamond-square-diamond rearrangement,<sup>41</sup> where the contact between the atoms in the groove opposite the missing cap atom is broken and a contact between the adjacent capping atoms is formed (compare the second views of the two structures in Fig. 3 and 4). During this process the two capping atoms are also drawn closer to the central atom to form new contacts, thus giving the central atom a coordination number of 14. The planes containing the two five-fold rings of atoms that were parallel in the Marks decahedron are now splayed apart (see the

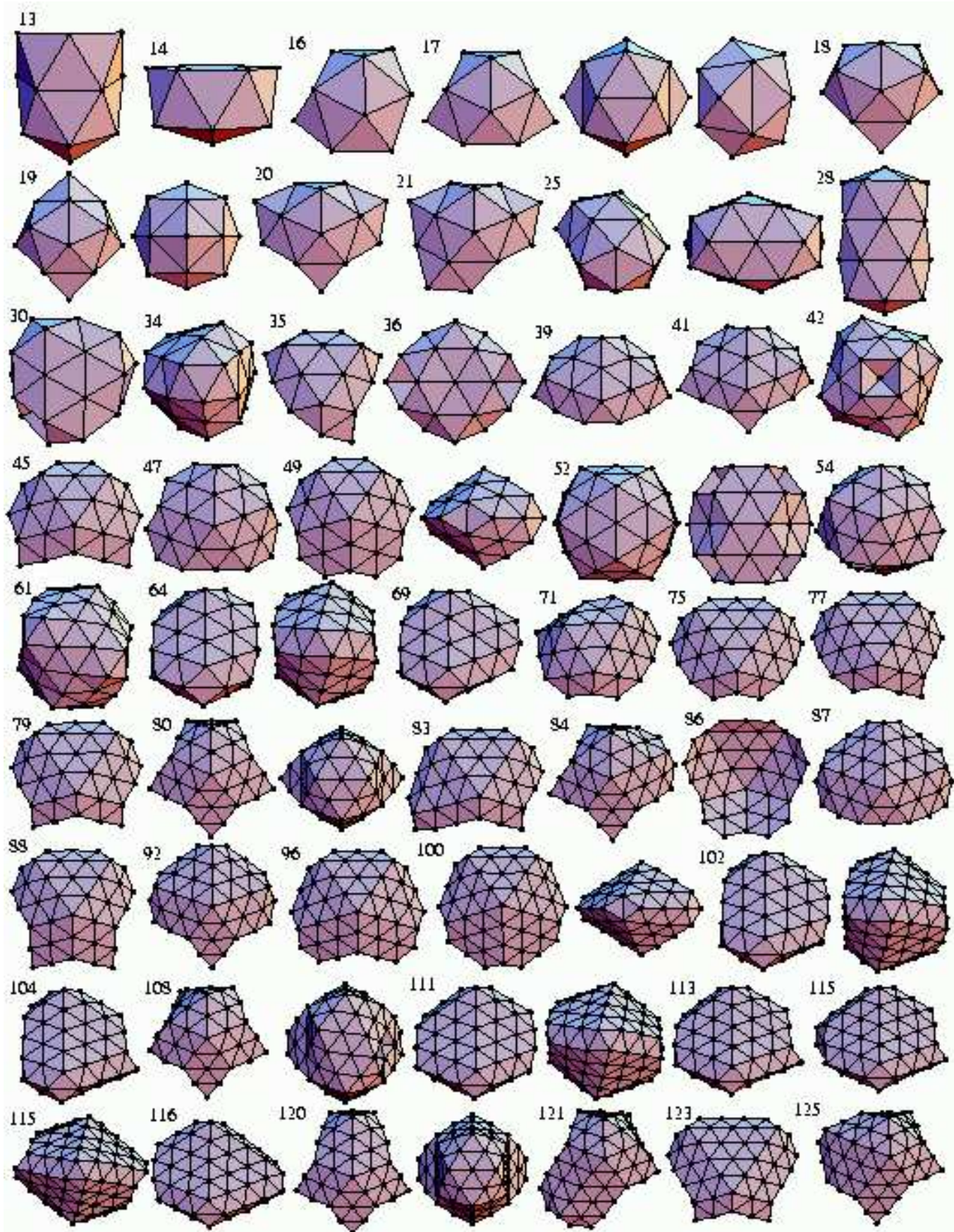


FIG. 3: A selection of the putative global minima for  $Zn_N$ .

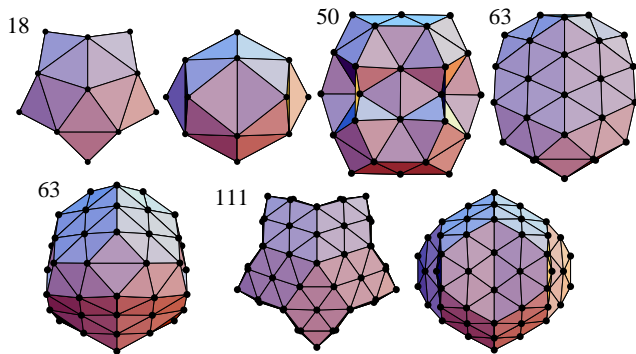


FIG. 4: A selection of reference structures for interpreting the  $Zn_N$  and  $Cd_N$  global minima.

third view of the  $Zn_{17}$  global minimum). It is also noticeable that the structure in the region of the distortion locally resembles the 13-atom icosahedron with the surface atoms now six coordinate.<sup>21</sup> The second view of  $Zn_{17}$  looks down a two-fold axis of this icosahedral-like region.

The energetic advantage provided through this ‘groove-bridging’ distortion is mainly through the lowering of the energies of the two capping atoms that come into contact. The increase in their coordination number to 6 gives rise to both an increase in  $\bar{\rho}$  and a more favourable pair energy. The energy of the central atom is left relatively unaffected, because the increase in coordination number is compensated by an increase in the average nearest-neighbour separation for that atom.

The other global minima for  $N=16-21$  can be also understood in terms of this distortion.  $Zn_{16}$  simply has one less capping atom than  $Zn_{17}$ . For  $N=18$  and 19 two of the grooves are bridged, giving rise to a 16-coordinate central atom. The combined effect of the two distortions also causes the contact in the groove adjacent to these two distortions to be broken, thus giving rise to a square face, which is itself capped in  $Zn_{19}$ , and a four-fold axis of symmetry (see the second view of  $Zn_{19}$ ).  $Zn_{20}$  and  $Zn_{21}$ , like  $Zn_{17}$ , are only distorted at one groove; the additional atoms fill in some of the other grooves taking the structure closer towards the 23-atom pentagonal bipyramid.

Such distorted decahedral structures have previously been seen for a number of metal potentials,<sup>10,13,14,21,36,42,43,44</sup> particularly those that have a tendency to disorder. Indeed, Soler *et al.* have identified such structures as particularly important for amorphous gold clusters, and have used them as a basis to suggest schemes to produce potentially new magic number clusters for larger sizes.<sup>21</sup>

As the size of the clusters increase, so of course must the number of atoms in the interior.  $Zn_{25}$  is typical of most of the clusters with two internal atoms. It can be considered as two interlocking distorted decahedra. In the view shown in Fig. 3 a  $Zn_{18}$ -like fragment can be clearly seen. The exception to these type of structures occurs at  $Zn_{28}$ . The six-fold symmetric structure is a continuation of  $Zn_{14}$  and has four stacked hexagonal rings

arranged in an antiprismatic fashion. One would expect such a structure to have three internal atoms, but instead there is a vacancy in the very centre of the structure. Again, this is to avoid internal atoms with values of  $\bar{\rho}$  that are too large.

$Zn_{30}$  and  $Zn_{34}$  are typical of structures with three and four internal atoms. The overall shape reflects the triangular and tetrahedral arrangement of the internal atoms, but it is again hard to detect any overall order.  $Zn_{36}$  provides an interesting exception. The surface atoms have basically the same geometry as a recently identified 38-atom polytetrahedral structure.<sup>19,20</sup> However, there are only four (not six) internal atoms, and these are arranged as a planar rhombus.

First at  $N=35$  and then from  $N=38$  a new series of distorted decahedral structures begins. Again they are based on a Marks decahedra that has been created from a pentagonal bipyramid (in this case with 54 atoms) by introducing reentrant grooves that are one layer deep. A similar mechanism of distortion is again seen. Atoms that are on the equatorial edges of the cluster either side of a groove are drawn closer together, although in this case a contact is not actually formed—the distortion is a diamond-square rather than a diamond-square-diamond process. The clusters at  $N=35, 39, 41, 45, 47$  and 49 in Fig. 3 provide examples of structures in this sequence. In most of the examples, two such distortions are present at adjacent grooves, and so the whole edge between these grooves is brought closer to the centre of the cluster, forming new contacts with the closest interior atoms. As can be seen for the second view of the complete 49-atom Marks decahedron, this lead to a splaying of the planes of pentagonal rings that would otherwise have been parallel.

For these larger clusters, these distortions represent a smaller perturbation on the overall structure than for  $N=16-21$ . Indeed, they are barely visible when the cluster is viewed down the quasi-fivefold axis. All that can be seen is a slight opening of the angle at the reentrant groove.

Comparing the energetics of the distorted and undistorted 49-atom Marks decahedron shows that the main improvement arising from the distortion is for the interior atoms. The movement of the equatorial edges involved in the distortion closer to the centre of the cluster compresses the rest of the surface somewhat and increases the coordination number of some of the interior atoms. This leads to a structure where the ratio of the nearest neighbour distances for the interior atoms to those of the surface atoms increases from 1.049 to 1.060. Thus, there is less need for the surface to shrink inwards and compress the core in order to improve the  $\bar{\rho}$  values of the surface atoms. Consequently,  $\bar{\rho}_{\text{bulk}}$ , the average  $\bar{\rho}$  value for the interior atoms, decreases from 9.197 to 8.756, i.e. closer to  $\bar{\rho}_{\text{xtal}}$ , and so the energy of the interior atoms decreases. By contrast the distortion has little overall effect on the energy of the surface atoms. Generally, the atoms in the equatorial plane, especially those close to the distortion, improve their energies, but many of the other

surface atoms lose out due to the breaking or stretching of contacts in the axial direction.

This decahedral series of structures is interrupted at  $N=42$  and  $43$  by structures with four-fold symmetry. These clusters are loosely related to the 44-atom fcc octahedron, but with one or two opposite vertices removed. The top half of the cluster is then twisted with respect to the bottom to give a slightly buckled outer layer.

Beyond  $N=50$  these groove-bridged Marks decahedra are no longer most stable. Instead, there is a size range where the structures typically have no overall order, but where motifs that resemble fragments of Marks decahedra and Mackay icosahedra are evident.  $Zn_{54}$  provides a typical example, whereas  $Zn_{52}$  is a structure with more order evident. From one side  $Zn_{52}$  has perfect Mackay icosahedral order. What has occurred to the other side can be determined by comparing to the 50-atom incomplete Mackay icosahedron shown in Fig. 4. The two contacts that complete the five-fold rings around the two empty vertices of the Mackay icosahedron have been broken, removing some of the tension in the outer layer of the Mackay icosahedron that makes it so energetically unfavourable.<sup>45</sup> Then two atoms (oriented horizontally with respect to the views in the figures) are inserted into the coordination shell of the central atom, increasing its coordination number. Such a structure has previously been located for  $Au_{52}$  modelled by a Sutton-Chen potential.<sup>10</sup>

From the particularly stable structures based on the 18-atom and 49-atom Marks decahedra, it is not surprising that there is another series of magic numbers leading to the 100-atom Marks decahedron. Again this Marks decahedron is formed from a pentagonal bipyramid by the introduction of grooves of depth one layer. More generally, one can use this trend to predict potential magic number clusters outside the size range of this study. The sizes for such complete Marks decahedra are given by

$$N = \frac{5}{6}n^3 + 5n^2 + \frac{61}{6}n + 2 \quad (14)$$

where  $n$  is the number of atoms on an equatorial edge of the Marks decahedron. This gives  $N=18, 49, 100, 176, 282, \dots$

The first of this set of groove-bridged decahedral structures occurs at  $N=75$  and the last at  $N=101$ . Representative examples at  $N=75, 77, 79, 83, 86-88, 92, 96$  and  $100$  are shown in Fig. 3. At the smallest sizes the decahedra are still quite asymmetric. From Fig. 2 one can see that the particularly stable sizes occur at  $N = 100 - 4m$ , where  $m=0-3$ . These structures can be formed from  $Zn_{100}$  by the sequential removal of 4-atoms from each groove to give structures that have  $m$  grooves that are two layers deep. It is interesting to know that the complete Marks decahedron is not in fact the most stable of these structures, but that a slight asymmetry is preferred.

Comparing the energetics of the 100-atom distorted and undistorted Marks decahedra reveals a similar story

to  $Zn_{49}$ . The main stabilization of the distorted structure is due to the decrease in  $\bar{\rho}_{\text{bulk}}$  from 8.875 to 8.789. It is also interesting to analyse the reasons for the stability of structures at  $N=88$  and  $92$  with four-coordinate surface atoms. Firstly, this is because a four-coordinate atom can compensate for its low coordination by having very short nearest-neighbour distances, thus achieving a reasonable  $\rho$  value; e.g. 7.519 for  $Zn_{92}$ . Secondly, this additional short contact reduces the need for the four surface atoms in contact with the adatom to shrink inward and compress the adjacent interior atoms. For  $Zn_{92}$  the  $\bar{\rho}$  values for these atoms only increase by 0.313, despite this extra contact, because the pair separations for the other six contacts have expanded by 2.5%.

The structures at  $N=63-70$  are also closely based on the 100-atom Marks decahedron, but with a further distortion. From the first view of  $Zn_{64}$  one can see the resemblance to the 63-atom structure in Fig. 4 that is an asymmetric fragment of the 100-atom distorted Marks decahedron. The second view of  $Zn_{64}$  shows the 2-fold axis. From the equivalent view of the 63-atom structure, it is clear that an extra atom has been added to the column of three capping atoms (at the bottom of the first view and in a vertical line in the centre of the top half of the cluster in the second view), and then a small twist has been given to the two halves of the structure.  $Zn_{69}$  has basically the same structure but with an increase in the size of one of the decahedral faces.

Based on the favourability of small distorted Marks decahedra (similarly to those we see at  $N=16-21$ ) for gold clusters modelled by a Gupta potential, Soler *et al.* suggested a means for using this structural pattern to generate potentially stable large clusters.<sup>21</sup> A 55-atom Mackay icosahedron can be generated from a 13-atom icosahedron by the addition of atoms at the centre of each nearest-neighbour contact. By the same process, an 80-atom structure can be generated from an 18-atom distorted Marks decahedron with one of the grooves bridged. Soler *et al.* envisaged that this structure would be most stable when the three four-coordinate atoms in this 80-atom structure were removed.<sup>21</sup> However, the suggested structure is actually the global minimum for  $Zn_{80}$ , reflecting the stabilization of low-coordinate atoms that is possible for this potential.

An alternative way to generate the  $Zn_{80}$  structure is to introduce reentrant grooves two layers deep into the 100-atom pentagonal bipyramid. This Marks decahedron is then distorted to produce four new contacts that bridge the two capping square pyramids adjacent to a groove. This distortion is analogous to that for bridging a groove one layer deep. In the region of the distortion, the structure looks locally like a 55-atom Mackay icosahedron.

Bridging a groove that is two layers deep is generally less favourable than bridging one that is one layer deep. There are only five examples for  $N \leq 100$ . The others occur for  $Zn_{71-73}$  and  $Zn_{84}$ .  $Zn_{71}$  and  $Zn_{84}$  are quite interesting because they involve distortions of grooves that are both one and two layers deep. For example,  $Zn_{84}$  can

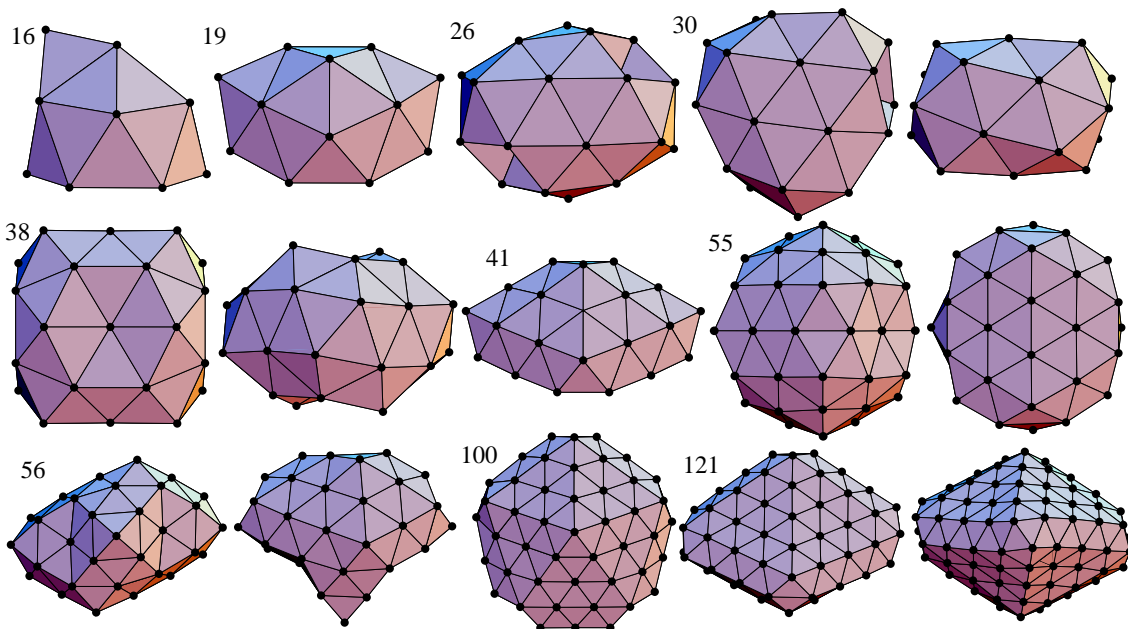


FIG. 5: A selection of the putative global minima for  $\text{Cd}_N$  that differ from those for  $\text{Zn}_N$ .

be formed from  $\text{Zn}_{80}$ , by first filling in one of the grooves, so that it is then only one layer deep and then applying the distortion to this groove.

After the completion of the previous decahedral series associated with the Marks decahedra at  $N=18$  and  $49$ , there are size ranges where the majority of clusters have no discernible overall order at  $N=22-34$  and  $N=51-62$ , before structures based on the next Marks decahedron become lowest in energy. However, even though the next complete Marks decahedron is at  $N=176$ , beyond  $N=101$  structures based on this larger Marks decahedron are immediately lowest in energy. From  $N=102-117$  (excepting  $N=108$ ) the zinc clusters are asymmetric groove-bridged decahedra with the same twist distortion as that for  $\text{Zn}_{64}$  this leads to structures with a two-fold axis of symmetry at  $N=111$  and  $115$  (see the second views of these structures in Fig. 4).

The first global minima that are fragments of the 176-atom Marks decahedron with only distortions bridging grooves one layer deep occur at  $N=122$  and  $123$ . There are also a number of structures, where grooves two layers deep are bridged; e.g.  $N=108, 120, 121$  and  $125$ . The structures at  $N=108, 121$  and  $125$  are slightly more complicated, because the reentrant  $\{111\}$  faces in the grooves of the undistorted Marks decahedra are not triangular but instead have two atoms along the outer apical edge. This is illustrated for  $\text{Zn}_{108}$ , which is based on the 111-atom Marks decahedron shown in Fig. 4. On bridging this groove, it is favourable to remove three atoms that lie on the  $\sigma_h$  mirror plane of the Marks decahedron, and to twist the top and bottom of the cluster slightly to remove a small  $\{100\}$ -type face that would otherwise result.

As has already been noted, for just over half the cad-

mium clusters in the size range considered, the global minimum have the same structures as the zinc clusters. A selection of examples where the global minimum differs from zinc are depicted in Fig. 5. The global minima are again dominated by distorted Marks decahedra, although the positions of capping atoms (e.g.  $\text{Cd}_{16}$  and  $\text{Cd}_{19}$ ) or the number of grooves that are bridged (e.g.  $\text{Cd}_{100}$ ) may be different. To take  $\text{Cd}_{100}$  as an example, this structure is second lowest in energy for zinc, because, although it has a better embedding energy than the global minimum, this is more than offset by a worse pair energy. However, because of the reduced magnitude of the pair interactions for cadmium this structure is now lowest in energy.

Another difference between the two systems is the more pronounced stability of the twisted Marks decahedra for cadmium, as indicated by Fig. 2 and the larger size ranges ( $N=63-72$  and  $102-121$ ) for which these structures are most stable. A further difference is that decahedral structures where grooves of depth two are bridged are less common—there are only three examples for cadmium clusters in the size range considered here.

The least coincidence between the zinc and cadmium global minima probably occurs in the size windows between the series of distorted Marks decahedra where the structures often have no overall order. This probably reflects the large number of disordered structures that only have small differences in energy. Examples of clusters from these size ranges with  $N=26, 30, 38, 55$  and  $56$  are shown in Fig. 5.

#### IV. CONCLUSION

I have analysed the structures of the global minima up to  $N=125$  for two metallic potentials that have been previously found to have a particularly strong tendency to exhibit disordered clusters. This study confirms that the clusters exhibit none of usual ordered forms for materials that are close-packed in bulk. Instead, the majority of the clusters are based on distorted oblate Marks decahedra, but where the distortions are well-defined. There are series of structures associated with the 18-, 49-, 100- and 176-atom complete Marks decahedra. However, in between there are size windows where the majority of the clusters have no overall order, except for  $N > 100$  where there is a direct transition between structures based on the 100- and 176-atom Marks decahedra.

Because the effective pair potentials of these zinc and cadmium potentials are very shallow, thus providing relatively little constraint on the pair separations, there is a strong tendency for the surface atoms to contract inwards in order for these atoms to obtain a better many-body embedding energy. The resulting compression of the interior of the cluster causes the conventional structures to be disfavoured,<sup>17</sup> because it results in a  $\bar{\rho}_{\text{bulk}}$  that is significantly larger than  $\bar{\rho}_{\text{xtal}}$ . Instead structures for which the nearest-neighbour distances for the surface atoms are naturally longer than those for the interior atoms are likely to be favoured, because this allows the difference between  $\bar{\rho}_{\text{bulk}}$  and  $\bar{\rho}_{\text{surf}}$  to be reduced, bringing them both closer to the optimal value. The distortions of the oblate Marks decahedra help to achieve just this.

This paper should be seen in the context of a growing research program that has sought to understand how the observed structures for metal clusters depend on the form of the many-body potential.<sup>11,17,38,46,47</sup> Even for simple potentials of the embedded-atom (or glue) form (Eq. 2) this leads to significant complexity. The current results further highlight how many-body potentials can lead to the stabilization of unusual structural forms.<sup>11,17,21,38,47</sup> Of course, at sufficiently large sizes the bulk structure, in this case hexagonal close-packed, should become most stable, but the energy differences found in this study sug-

gest that the current clusters are far from this limit.

The emphasis in this paper has been on the zinc and cadmium clusters as model systems with a strong tendency to disorder. As noted in Sect. II A, with the Gupta potential it is difficult to capture the large  $c/a$  ratio for Zn and Cd without introducing discrepancies for other properties. I have also performed a brief set of global optimization runs using Cleri and Rosato's alternative Gupta potential for Cd, where the  $c/a$  ratio was allowed to vary during the fitting. For the selection of sizes I tested the usual ordered forms, i.e. close-packed, icosahedral and decahedral, were always most stable. Reyes-Nava *et al.* also found these cadmium clusters to have strong first-order-like melting transitions, again reflecting the strong ordering for this alternative potential.<sup>48</sup> Given this strong dependence on the potential parameterization, one should be somewhat sceptical about the abilities of these potentials to provide realistic models for zinc and cadmium clusters. However, the tendency to disorder for these clusters seems to be reproduced by electronic structure calculations using density-functional theory.<sup>7</sup>

There has been little other relevant work. Experiments on these clusters have focussed on their electronic shell structure,<sup>49,50</sup> rather than their geometries, and there are only a few theoretical studies to go beyond very small sizes. For cadmium clusters electronic structure calculations have been performed up to 20 atoms.<sup>51</sup> These found Cd<sub>13</sub> to be an icosahedron and the larger clusters to be based upon this structure.<sup>51</sup> Ramprasad and Hoagland studied zinc clusters using a many-body potential of the embedded-atom form (Eq. 2), but where the effective interactions looked very different from the current Gupta potential.<sup>52</sup> Of the series of candidate structures that they reoptimized, they also found icosahedral structures to be lowest in energy.

#### Acknowledgments

The author is grateful to the Royal Society for the award of a University Research Fellowship.

\* jpkd1@cam.ac.uk

<sup>1</sup> J. P. K. Doye, D. J. Wales, and R. S. Berry, *J. Chem. Phys.* **103**, 4234 (1995).

<sup>2</sup> J. P. K. Doye and D. J. Wales, *J. Chem. Soc., Faraday Trans.* **93**, 4233 (1997).

<sup>3</sup> I. L. Garzón, K. Michaelian, and M. R. Beltrán, *Phys. Rev. Lett.* **81**, 1600 (1998).

<sup>4</sup> K. Michaelian, N. Rendón, and I. L. Garzón, *Phys. Rev. B* **60**, 2000 (1999).

<sup>5</sup> I. L. Garzón, C. Rovira, K. Michaelian, M. R. Beltrán, P. Ordejón, J. Junquera, D. Sanchez-Portal, E. Artacho, and J. Soler, *Phys. Rev. Lett.* **85**, 5250 (2000).

<sup>6</sup> A. Taneda, T. Shimuzu, and Y. Kawazoe, *J. Phys.-*

*Condens. Mat.* **13**, L305 (2001).

<sup>7</sup> K. Michaelian, M. R. Beltrán, and I. L. Garzón, *Phys. Rev. B* **65**, 041403(R) (2002).

<sup>8</sup> I. L. Garzón, K. Michaelian, M. R. Beltrán, A. Posada-Amarillas, P. Ordejón, E. Artacho, D. Sánchez-Portal, and J. Soler, *Eur. Phys. J. D* **9**, 211 (1999).

<sup>9</sup> M. D. Glossman, J. A. Alonso, and M. P. Iñiguez, *Phys. Rev. B* **47**, 4747 (1993).

<sup>10</sup> J. P. K. Doye and D. J. Wales, *New J. Chem.* **22**, 733 (1998).

<sup>11</sup> J. P. K. Doye and S. C. Hendy, *Eur. Phys. J. D* **22**, 99 (2003).

<sup>12</sup> J. Oviedo and R. E. Palmer, *J. Chem. Phys.* **117**, 9548

- (2002).
- <sup>13</sup> N. T. Wilson and R. L. Johnston, *Eur. Phys. J. D* **12**, 161 (2000).
- <sup>14</sup> S. Darby, T. V. Mortimer-Jones, R. L. Johnston, and C. Roberts, *J. Chem. Phys.* **116**, 1536 (2002).
- <sup>15</sup> C. Massen, T. V. Mortimer-Jones, and R. L. Johnston, *J. Chem. Soc., Dalton Trans.* pp. 4375–4388 (2002).
- <sup>16</sup> J. Wang, G. Wang, and J. Zhao, *Phys. Rev. B* **66**, 035418 (2002).
- <sup>17</sup> J. M. Soler, M. R. Beltrán, K. Michaelian, I. L. Garzón, P. Ordejón, D. Sánchez-Portal, and E. Artacho, *Phys. Rev. B* **61**, 5771 (2000).
- <sup>18</sup> D. J. Wales, *Chem. Phys. Lett.* **285**, 330 (1998).
- <sup>19</sup> J. P. K. Doye, D. J. Wales, and S. I. Simdyankin, *Faraday Discuss.* **118**, 159 (2001).
- <sup>20</sup> J. P. K. Doye, D. J. Wales, F. H. Zetterling, and M. Dzugutov, *J. Chem. Phys.* **118**, 2792 (2003).
- <sup>21</sup> J. M. Soler, I. L. Garzón, and J. D. Joannopoulos, *Solid State Commun.* **117**, 621 (2001).
- <sup>22</sup> R. P. Gupta, *Phys. Rev. B* **23**, 6265 (1981).
- <sup>23</sup> F. Cleri and V. Rosato, *Phys. Rev. B* **48**, 22 (1993).
- <sup>24</sup> R. A. Johnson and D. J. Oh, *J. Mater. Res.* **4**, 1195 (1989).
- <sup>25</sup> F. Ercolessi and J. B. Adams, *Europhys. Lett.* **26**, 583 (1994).
- <sup>26</sup> H. S. Lim, C. K. Ong, and F. Ercolessi, *Surf. Sci.* **269/270**, 1109 (1992).
- <sup>27</sup> Y. Mishin, D. Farkas, M. J. Mehl, and D. A. Papaconstantopoulos, *Phys. Rev. B* **59**, 3393 (1999).
- <sup>28</sup> D. J. Wales and J. P. K. Doye, *J. Phys. Chem. A* **101**, 5111 (1997).
- <sup>29</sup> D. J. Wales and H. A. Scheraga, *Science* **285**, 1368 (1999).
- <sup>30</sup> Z. Li and H. A. Scheraga, *Proc. Natl. Acad. Sci. USA* **84**, 6611 (1987).
- <sup>31</sup> C. J. Tsai and K. D. Jordan, *J. Phys. Chem.* **97**, 11227 (1993).
- <sup>32</sup> F. H. Stillinger, *Phys. Rev. E* **59**, 48 (1999).
- <sup>33</sup> J. P. K. Doye and D. J. Wales, *J. Chem. Phys.* **116**, 3777 (2002).
- <sup>34</sup> D. J. Wales, J. P. K. Doye, A. Dullweber, M. P. Hodges, F. Y. Naumkin, F. Calvo, J. Hernández-Rojas and T. F. Middleton, The Cambridge Cluster Database, <http://www-wales.ch.cam.ac.uk/CCD.html>.
- <sup>35</sup> J. P. K. Doye, M. A. Miller, and D. J. Wales, *J. Chem. Phys.* **111**, 8417 (1999).
- <sup>36</sup> S. K. Lai, P. J. Hsu, K. L. Wu, W. K. Liu, and M. Iwamatsu, *J. Chem. Phys.* **117**, 10715 (2002).
- <sup>37</sup> J. P. K. Doye, unpublished.
- <sup>38</sup> J. P. K. Doye, *J. Chem. Phys.* p. in press (2003).
- <sup>39</sup> In many cases, although not for the presents clusters, to produce particularly stable Marks decahedra, as well as the introduction of grooves into the pentagonal bipyramids, it is also important to truncate the equatorial edges to reveal {100} facets.
- <sup>40</sup> L. D. Marks, *Philos. Mag. A* **49**, 81 (1984).
- <sup>41</sup> W. N. Lipscomb, *Science* **153**, 373 (1966).
- <sup>42</sup> L. D. Lloyd and R. L. Johnston, *Chem. Phys.* **236**, 107 (1998).
- <sup>43</sup> L. D. Lloyd and R. L. Johnston, *J. Chem. Soc., Dalton Trans.* pp. 307–316 (2000).
- <sup>44</sup> A. Sebetci and Z. B. Güvenc, *Surf. Sci.* **525**, 66 (2003).
- <sup>45</sup> The 55-atom Mackay icosahedron is in fact 0.828 eV higher in energy than the  $Zn_{55}$  global minimum.
- <sup>46</sup> F. Baletto, R. Ferrando, A. Fortunelli, F. Montalenti, and C. Mottet, *J. Chem. Phys.* **116**, 3856 (2002).
- <sup>47</sup> S. C. Hendy and J. P. K. Doye, *Phys. Rev. B* **66**, 235402 (2002).
- <sup>48</sup> J. A. Reyes-Nava, I. L. Garzón, and K. Michaelian, *Phys. Rev. B* **67**, 165401 (2003).
- <sup>49</sup> I. Katakuse, T. Ichihara, Y. Fujita, T. Matsuo, T. Sakurai, and H. Matsuda, *Int. J. Mass. Spectrom.* **69**, 109 (1986).
- <sup>50</sup> M. Ruppel and K. Rademann, *Chem. Phys. Lett.* **197**, 280 (1992).
- <sup>51</sup> J. Zhao, *Phys. Rev. B* **64**, 043204 (2001).
- <sup>52</sup> R. Ramprasad and R. G. Hoagland, *Modelling Simul. Mater. Sci. Eng* **1**, 189 (1993).